Suppression of eddy-current effects in beam injection using a pulsed sextupole magnet with a new ceramic chamber

Chikaori Mitsuda,* Hiroyuki Takaki, Ryota Takai, Takashi Nogami, Takashi Uchiyama, Yukinori Kobayashi, and Takashi Obina

Accelerator Laboratory, High Energy Accelerator Research Organization (KEK), Tsukuba, Ibaraki 305-0801, Japan

Yao Lu

The Graduate University for Advanced Studies, SOKENDAI, Hayama, Kanagawa 240-0193, Japan

Atsushi Yokoyama

KYOCERA Co. Ltd., Higashiomi, Shiga 529-1595, Japan

(Received 1 June 2022; accepted 7 November 2022; published 29 November 2022)

At the Photon Factory storage ring (PF ring) of the High Energy Accelerator Research Organization (KEK), a pulsed sextupole magnet (PSM) has been used for top-up injection for the first time. Following its successful operation at the KEK, this new injection scheme was expanded to one with a nonlinear kicker in BESSY II and was then applied at UVSOR and Aichi SR in Japan. Also, the PSM system in the PF ring was improved by introducing a rectangular shape for the magnet's bore to strengthen the magnetic field. However, this upgraded PSM was not implemented for user operation because it induced a horizontal oscillation of the stored beam with a maximum amplitude of 5.0 mm. This oscillation was assumed to be caused by eddy currents originating from the uniform inner coating of the ceramic chamber. We, therefore, developed a modified ceramic chamber with a new patterned coating designed to suppress the eddy current–induced magnetic field. The pattern shape was optimized to suppress this magnetic field and, simultaneously, to reduce the resistive wall impedance. A fine-line pattern-coating process, originally developed for a ceramic chamber with an integrated pulsed magnet, was modified for application with the magnet's chamber of the sextupole. The maximum horizontal oscillation amplitude was suppressed by a factor of 16 by using the new PSM chamber without any issues related to beam instability. Details of the historical background of the upgrading of the PSM system, an investigation of the cause of the abnormal oscillation problem, the development of the new process for coating the ceramic chamber, and the results of the beam-response measurements for the new ceramic chamber installed in the PF ring are reported in this article.

DOI: 10.1103/PhysRevAccelBeams.25.112401

I. INTRODUCTION

We have developed a new technique for top-up injection, which is indispensable for the stable supply of synchrotron radiation at the Photon Factory storage ring (PF ring) at the High Energy Accelerator Research Organization (KEK). This injection technique for stored beams uses a pulsed sextupole magnet; this was the first of its kind and was successfully operated at KEK. The technique has since been adapted into a multipole pulsed-magnet unperturbed-injection technique by using a nonlinear magnetic field kicker in BESSY II [1] and the injection technique with a pulsed sextupole magnet was applied at UVSOR [2] and Aichi SR [3] in Japan following its success in KEK. The unperturbed injection technique is a candidate for use as a top-up injection technique for the next generation of synchrotron radiation sources with ultralow emittances.

Because top-up injection has recently become common, the axis of the synchrotron radiation beam axis needs to remain stable during beam injection; this requires that the stored-beam orbit does not oscillate. Injection using pulsed multipole magnets does not require the bump orbit that is used in conventional injection and, therefore, does not require the precise similarity and synchronization of the waveforms of the pulsed power supplies. The technique also eliminates the problem of incomplete closure of the bump orbit when magnets that create nonlinear magnetic fields are present in the bump orbit. Moreover, synchrotron radiation beamlines with bending magnets

*chikaori.mitsuda@kek.jp

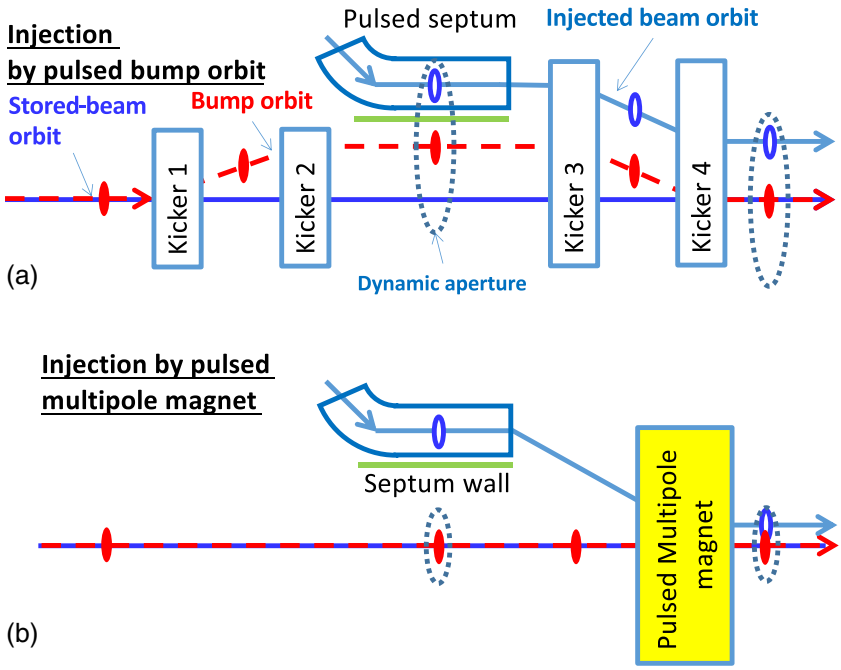

FIG. 1. Comparison of injection schemes using a conventional pulsed bump orbit (A) and a pulsed multipole magnet (B). The dynamic aperture is indicated schematically to illustrate the merging of the injection beam into the narrow dynamic aperture.

can be constructed in the injection section. The requirement for only one pulsed magnet also saves space in the injection section. In addition, with bump injection, the initial amplitude is determined by the distance from the injection beam to the bump orbit on the other side of the septum wall [Fig. 1(a)]; in contrast, the amplitude of the oscillation of the injection beam is determined by the position and angle of the injection beam at the location of the pulsed multipole magnet [Fig. 1(b)]. Injection using pulsed multipole magnet should also facilitate merging of the injection beams into the small dynamic aperture of the next generation of the light sources (Fig. 1).

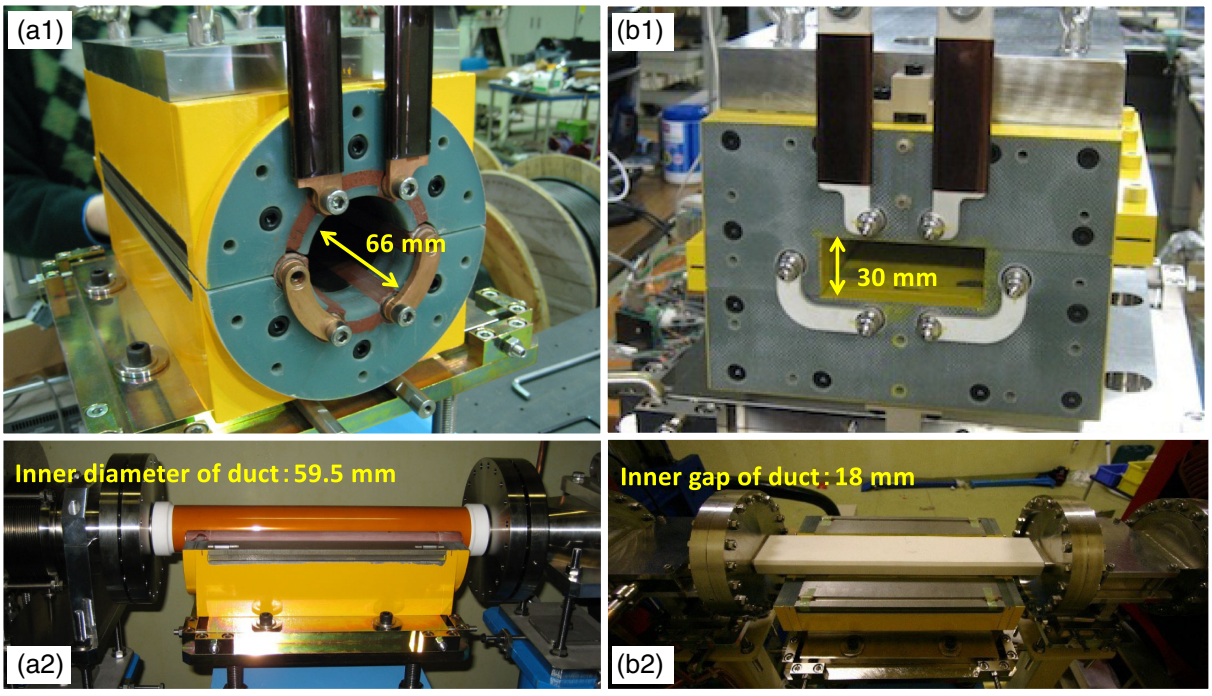

FIG. 2. Photographs of the magnets and ceramic chambers of PSM1 (A-1, A-2) and PSM2 (B-1, B-2).

The development of the multipole pulsed magnet injection technology at KEK began with the successful demonstration of 3-GeV beam injection using a pulsed quadrupole magnet (PQM) at the Photon Factory Advanced Ring (PF-AR) in 2005 [4]. In 2006, the development of a pulsed sextupole magnet (PSM) began. Top-up injection using a PSM was first demonstrated in 2008 [5] and was subsequently adopted for user operation from 2010 to 2014, although the operation was interrupted for 6 months by the 2011 Tohoku Earthquake off the Pacific coast of Japan.

In 2014, the PSM system was upgraded to solve operational issues with both the power supply and the magnet; the system before 2014 is referred to as PSM1, and the system after 2014 is referred to as PSM2. To increase the kick angle at an off-center position of the magnet, the gap was narrowed and its shape was changed to a rectangular one to secure a horizontal physical aperture (Fig. 2). The scale of the horizontal aperture was expanded from 66 to 80 mm, and the physical aperture was fixed at 68 mm in the inside of the ceramic vacuum chamber. Because PSM1 was powered by a recycling power supply, the pulse width of the output current was 2.4 μs, which corresponds to 4 times the beam revolution time of 624 ns. The pulse width of the power supply for PSM2 was shortened to 1.2 μs to reduce the multiturn kick. The maximum voltage was also increased from 33 to 35 kV to enhance the strength of the magnetic field. However, the operation of the PSM2 system was discontinued after its installation in 2014 because it induced a horizontal oscillation with a maximum amplitude of 5 mm on the stored beam, which adversely affected the injection efficiency. The aim of our study was to solve the problem of oscillation of the stored beam in the PSM2 system.

II. UPGRADE OF THE PSM SYSTEM

A. Existence of an unexpected magnetic field at the center of the magnet

Because the magnetic-field distribution of a sextupole magnet has a parabolic shape, there is a point at the center of the magnet where the magnetic field is zero and a region where it approximates to zero. If the center of magnetic field is precisely aligned with the orbit of the stored beam, the magnetic field does not affect the stored beam; it affects only the injected beam, which passes through an off-center position of the magnet. The injection beam orbit with an injection angle is then parallel to the stored-beam orbit in the storage ring after receiving a kick from a pulsed magnetic field so that the injection beam becomes closer to the stored beam. However, the stored beam at the center of the magnetic field was found to undergo marked oscillations during beam experiments using PSM2.

Although a slight horizontal oscillation was observed during operation of the PSM1, the absence of a quadrupole magnetic field resulted in a marked improvement in the "blink" of the beam compared with that of beam injection using the PQM. The effect of the pulsed multipole magnet injection system was thus sufficiently demonstrated. However, the oscillation was more pronounced in the PSM2 system, which generated 28 times the oscillation amplitude of the PSM1 system. Table I shows a comparison of the magnet specifications, the maximum amplitude of the horizontal stored-beam oscillation at injection, and the measured pulsed magnetic field at the center of the magnet into which the ceramic chamber was inserted. The measured residual integrated magnetic fields of PSM1 and PSM2 are shown with excitation currents of 3000 and 2500 A, respectively, as used during the beam experiments. These currents correspond to the integrated magnetic field of 12 mTm at a horizontal position of 15 mm for a 2.5-GeV electron beam, which provides the required kick angle to merge the injection beam into the stored beam. For both PSM1 and PSM2, the unexpected magnetic field was estimated from the measured beam-oscillation amplitude when the old power supply was used for PSM1, whereas, the new power supply was used for PSM2. The difference in the excitation currents was due to the enhancement of the magnetic-field strength by narrowing of the gap; there was no difference in the structure except for the differences in the shape and dimensions of the gap. A rectangular shape was adopted to enhance the magnetic-field strength by narrowing the gap while maintaining a horizontal aperture, and the vertical gap dimension was reduced to $1/3.3$ of that of the circular shape. Moreover, the pulsed current width was shortened by a factor of 2 as a result of updating the power supply.

TABLE I. Horizontal oscillation amplitudes at injection for PSM1 and PSM2, along with their specifications.

Specification/magnet	PSM1	PSM2
Bore/gap (mm)	66.0	30.0
Inner diameter/width of the chamber (mm)		
Horizontal	59.5	68.0
Vertical	59.5	18.0
Coating thickness inside the chamber (μm)	3–5	
Thickness of lamination steel (μm)	150	
Thickness of insulation material between lamination steels (μm)	6	
Maximum oscillation amplitude (mm)	0.18	5.0
Pulsed current width (μs)	2.4	1.2
Residual field at magnet center (mT m)	0.15	4.2

The increase in the oscillation amplitude can be simply explained in terms of the combined effects of the reduced gap size and the increased pulsed current frequency. This explanation suggests the existence of an unexpected magnetic field that affects the stored-beam orbit as the gap size is narrowed. In fact, the PSM2 magnetic field for the magnet alone, without the ceramic chamber was measured

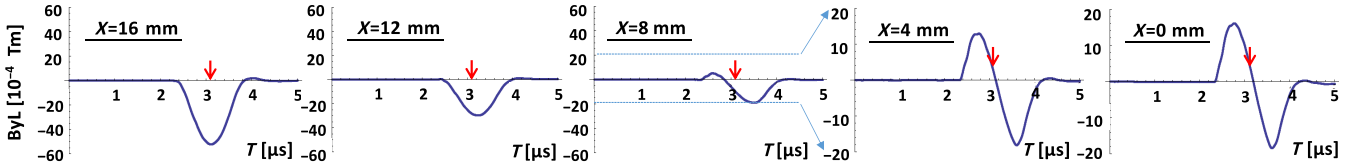

FIG. 3. PSM2 magnetic-field shape at each position in the magnet gap along the horizontal axis with the ceramic chamber. The red arrows show the timing of the kicking of the injected beam. The vertical axes for $x = 4$ mm and $x = 0$ mm are magnified by a factor of 3.

before the installation of PSM2 into the PF ring in 2014 because there was no suspicion of any issue relating to the ceramic chamber. After the discovery of the problem with PSM2, we reinvestigated and reanalyzed the magnetic-field distributions of PSM1 and PSM2 with the ceramic chamber in the present work. Notably, we carefully reviewed both the strength and the waveform of the magnetic field. As a result, in both PSM1 and PSM2, we identified a pulsed magnetic field that opposed the main field. Normally, such a pulsed magnetic field should not exist at the center of a magnet if a sextupole magnetic field is present.

B. Nature of the unexpected magnetic fields and their origin

The nature of the unexpected magnetic field can be understood by analyzing the raw signal data for the magnetic-field measurements at the center of the magnet. Figure 3 shows a single shot of the integrated magnetic-field waveform obtained by using an oscilloscope with a search coil which is sufficiently longer than the length of the magnet when the vertical magnetic field was measured along the horizontal axis in the midplane of the gap with the ceramic chamber inserted in the PSM2 magnet. The supplied voltage was set to be 10 kV, corresponding to an excitation current of 1074 A. The ByL of the label of the vertical axis in the figure is the strength of the vertical magnetic field integrated by the effective length of the magnet unless otherwise noted in this paper. At an off-center position far from the magnet's center, the magnetic-field waveform is the same as the excitation-current waveform; however, closer to the magnet's center, the amplitude gradually decreases and a waveform similar to a sine waveform appears without the magnetic-field strength going to zero. The timing of the kicking of the injected beam is indicated by the red arrows in the figure. Figure 4 shows the waveforms of a magnetic field for PSM2 at a position 15 mm from the center of the magnet with and without the ceramic chamber inserted in the gap. Under these conditions, the supplied high voltage was set to 25 kV, corresponding to a current of 2686 A. The insertion of the ceramic chamber attenuated the magnetic field by approximately 20% and delayed the appearance of the magnetic field by 132 ns.

The difference in the shape of the sinusoidal irregular field compared with that of the half-sine waveform of the supplied current (Fig. 3) and the delay caused by the ceramic chamber relative to the supplied current (Fig. 4) are typical results for magnetic fields generated by eddy-current effects. Figure 5 shows additional evidence of the presence of an eddy-current magnetic field. The amplitude of the eddy-current magnetic field increased linearly in response to a change in the supplied high voltage (Fig. 5). At the center of the magnet, the eddy-current magnetic field was more pronounced because of the absence of the sextupole magnetic field, which was the main magnetic field. Off-center from the magnet, a transition from a region where the eddy-current magnetic field was mixed with the sextupole magnetic field to a region dominated by the sextupole field was observed (Fig. 3). The reverse magnetic field, which interferes with the main magnetic field because of eddy currents, causes a delay and attenuation of the main field. These effects lead to a reduction in the kick angle for the injected beam. The arrows in Fig. 3, adjusted to the kicking timing of the injection beam, correspond to the nodes of the sine waveform when the stored beam at the center of the magnet was a single-bunch filling operation; therefore, the stored beam on this timing was not affected by the eddy current–induced

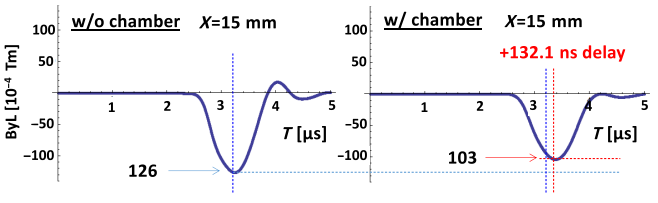

FIG. 4. Strength reduction and timing delay as a result of the effects of eddy currents in a pulsed field. The pulse width of the half-sine waveform with the chamber widened from 1.2 to 1.5 μs compared with the case without the chamber.

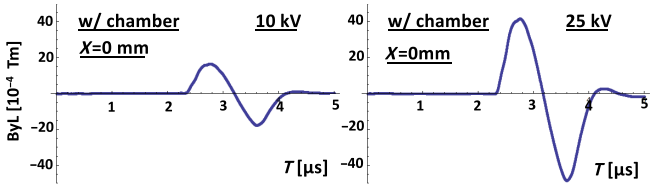

FIG. 5. The dependence of the eddy-current magnetic field on the supplied voltage.

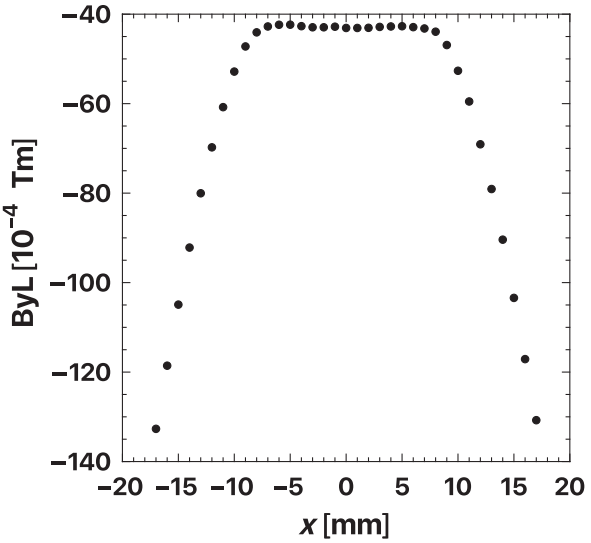

FIG. 6. Integrated magnetic field distribution for the horizontal axis when the ceramic chamber is inserted into the magnetic bore.

magnetic field. In the case of a multibunch filling operation, the stored beam exists at every timing on the waveform; consequently, the stored beam oscillated horizontally during the beam-injection period even if it passes through the center of the sextupole magnet. That is, the maximum amplitude of this sine waveform is the magnetic field that is the basis of the integrated magnetic field strength in Table I, and it is actually distributed uniformly over a wide area of ±8 mm from the center of the magnet's aperture (Fig. 6). These results shown in Fig 6 are based on the average of ten data points obtained by measuring the magnetic field of PSM2 and normalizing the results by the excitation current used in the beam experiment.

The expected amplitude of the horizontal beam oscillation is 6.9 mm, as calculated from the integrated field of -43×10^{-4} Tm by measurement of the magnetic field (see Fig. 6). This result is approximately consistent with the actual maximum amplitude of the horizontal beam oscillation (5 mm), if we consider that the timing of the stored beam with a single bunch is close to the node and not to the top of the sine waveform (Fig. 3). Furthermore, the stored beam clearly kicked a number of times because the width of the sine waveform of the eddy-current magnetic field increases to 1.8 μs compared with 1.2 μs corresponding to twice the beam revolution time. Notably, a sine waveform of the eddy-current magnetic field was also observed at the center of the magnet in the magnetic-field measurement in the absence of the ceramic chamber (Fig. 7). A simple comparison of the amplitudes of the sine waveforms suggests that the ratio of the strength of the eddy-current magnetic fields at the center of the magnet with and without the ceramic chamber was approximately 8∶1. We, therefore, inferred that the metal coating on the inner surface generated the eddy currents in the ceramic chamber and

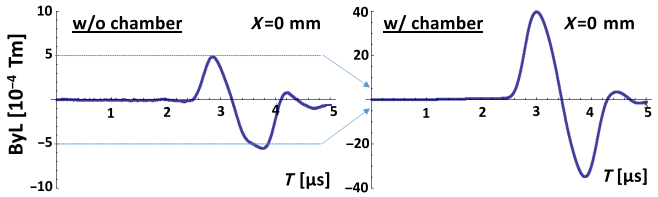

FIG. 7. Eddy-current effects of the magnet, as observed without a chamber installed in the bore. The left-hand figure shows the eddy-current signal of the magnet in the absence of the chamber. The right-hand figure shows the eddy-current signal, including eddy currents from the magnet and the chamber coating, in the presence of the chamber. Notably, the pulse width of the eddy-current signal in the absence of the chamber was shortened to 1.6 μs from 1.8 μs in the presence of the chamber.

that the iron core or coil generates the eddy currents in the magnet.

In PSM1, the beam injection was conducted smoothly, although the effect of an unexpected magnetic field due to eddy currents was observed. The oscillation of the stored beam in PSM1 had a maximum amplitude of 0.18 mm due to the eddy-current magnetic field; these oscillations were not sufficiently large to cause problems during user operation. PSM2, however, produced stored-beam oscillations with a maximum amplitude of 5 mm and was, therefore, not acceptable for user operations. The measured eddy-current magnetic field of PSM1 was 1/28 of that of PSM2 (see Table I), consistent with the observation that the ratio of the maximum amplitudes of their stored-beam oscillations of PSM1 and PSM2 was also 1/28. However, given that the ratio of the gaps between the magnets was 1/3.3 and that the frequency of the pulsed current of the new power supply was increased by a factor of 2.0 (from 2.4 μs to 1.2 μs), the eddy-current magnetic field generated in PSM1 was expected to be approximately 1/6.6 of that generated in PSM2 (the factor of 6.6 was estimated by multiplying 2.0 and 3.3). However, the actual stored-beam oscillation was even more suppressed than expected. Although the reason for this greater suppression of the oscillation has not been clearly identified, the mechanism of generation of the eddy-current magnetic field is expected to be correlated with the shape factors of, for example, the iron pole and ceramic chamber. The unexpected magnetic field generated in PSM1, as evaluated on the basis of magnetic-field measurements, has been discussed in detail elsewhere [6].

C. Measures to reduce eddy-current magnetic fields

The magnetic-field-permeable ceramic chamber has a thin titanium coating with a thickness of 3–5 μm to ensure the conduction of the beam-wall current and to suppress the eddy currents as much as possible. The titanium coating is much thinner than the skin depth of 411 μm assumed for the pulse width of the pulsed excitation current of the

sextupole magnet; consequently, the generation of eddy currents is suppressed. We prioritized the suppression of eddy-current generation by making the coating thinner, although this resulted in a higher volume resistance for the beam-wall current and adversely affected the beam impedance. The combined results of the magnetic-field measurements and beam experiments reveal that the thin-film coating causes a magnetic field due to eddy currents of non-negligible strength and that this field attenuated the main magnetic field to 80%, thereby causing oscillation of the stored beam. Because of the narrowing of the gap, the surface of the coating was close to the beam, which is likely to have strengthened the effect of the eddy current on the magnetic field. The rectangular-shaped bore has been adopted at UVSOR and Aichi SR, where the pulsed sextupole injection technique was adopted following the successful operation of the PF ring. In both facilities, oscillations of the stored beam, which should have been free of oscillations, were observed [7]. Suppression of the eddy-current effect is therefore considered an important issue for the establishment of pulsed multipole injection technology.

To identify the cause of this problem, we developed a new coating aimed at suppressing the generation of eddy current originating from the coating of the ceramic chamber, which was the main source of the irregularities in the magnetic field. According to the estimate from the content ratio of the eddy-current magnetic fields between the iron core and the coating, about 90% of eddy currents might be suppressed if the inner coating was improved. Instead of a full surface coating, it was necessary to develop a new coating technique that simultaneously suppresses eddy-current generation and enhances beam-wall current conductivity.

For the PF ring, an air-core-type ceramics chamber with an integrated pulsed magnet (CCiPM) [8] was developed as a pulsed multipole injection technique with an order higher than octupole, in parallel with the improvement of the injection techniques for the pulsed sextupole magnet. To this end, a new coating technology for the inner surface of the ceramic chamber was developed because of the limitations of the structures of the magnet coils implanted in the ceramic chamber and the need to suppress the eddy-current magnetic field. The new coating technology is referred to as the fine-line pattern-coating process (FLiP) and is one of the key technologies for the development of the CCiPM. The FLiP permits the implementation of a coating shaped like a fine-toothed comb; this does not generate large eddy-current loops in the longitudinal direction while providing a capacitance shape that permits the passage of the beam-wall currents. Moreover, the FLiP can be applied to the inner surface of ultrasmall-diameter ceramics with a diameter (ϕ) of as little as 30 mm.

The need for eddy-current suppression in kickers to prevent the attenuation of pulsed magnetic fields has long been discussed, and several techniques have been developed to achieve this. Typical examples include the strip or slit-shaped coatings that are used to suppress eddy currents in the kickers at the LHC [9] and SNS [10] hadron accelerators. Recognizing the usefulness of the improvement achieved with such coating geometries, we have been developing coating technologies with new geometries and structures of comb-shaped teeth. In particular, in the multibunch filling mode of the stored electron beam of the lepton accelerator (a synchrotron radiation source accelerator), marked adverse effects on the beam occur as a result of kicking by eddy current–induced magnetic fields generated at unexpected delay times and at positions other than that of the main pulsed magnetic field. The coating structure of the comb teeth is unlike any of those previously examined in research on hadron accelerators. In particular, the inner ceramic coating shows a distinct capacitance between the comb tooth, which face one another; it also has distinct electrical properties arising from the thin metallic coating on the ceramic surface of the dielectric, which has its own structural and electrical characteristics.

The application of this technology to the ceramic chamber of a pulsed sextupole magnet with a vertical gap of 18 mm is an important starting point for this development.

III. OPTIMIZATION OF THE CHAMBER'S INNER COATING

A. Optimization for eddy-current suppression

To optimize the comb-tooth shape for PSM2, various parameters related to the following shape dimensions can be varied: (i) the spacing between adjacent comb teeth, (ii) the width of the comb teeth, and (iii) the spacing at the end where the comb teeth face each other. From the viewpoint of eddy-current suppression, there is a boundary condition that the thickness of the comb-tooth-shaped coating should be below a certain value so that the comb teeth do not have a sufficiently large area to permit the generation of eddy currents. In addition, the gap between the comb teeth should not couple with the frequency of the pulsed excitation current; therefore, if the size of the gap of the order of a few millimeters, the resultant insulation effect will prevent the generation of large loops of eddy currents. In other words, because small eddy currents are localized as an individual cell on the plane of the comb-tooth-shaped coating, they cannot eventually integrate to form large eddy-current loops. However, care should be taken when considering the optimization of the comb-tooth shape, because small eddy currents are still present in the comb teeth, even if a large eddy-current loop is suppressed. From these perspectives, we optimized the geometry of the comb-tooth-shaped coating [11].

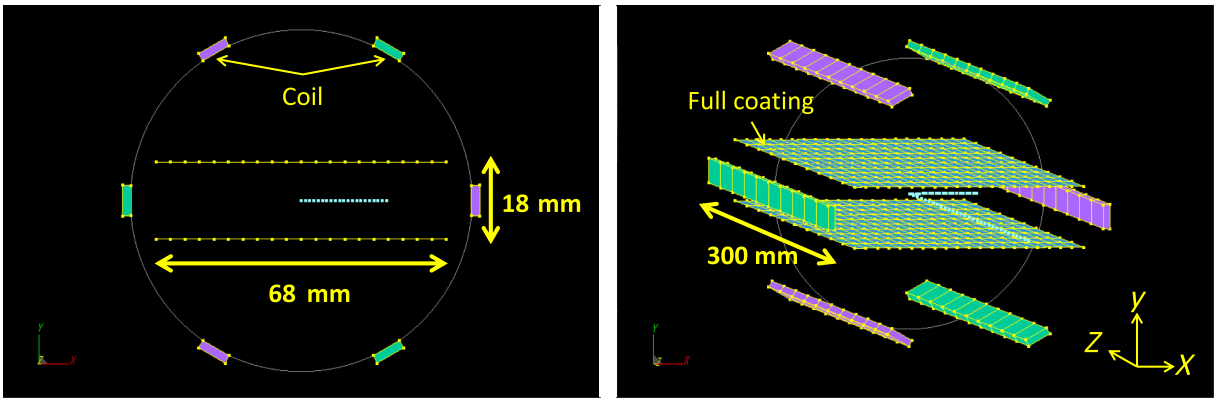

FIG. 8. Magnet modeling to optimize the parameters of the comb-tooth-shaped coating. The left-hand figure shows the cross-sectional structure of the coil and coating plate. The right-hand figure shows a three-dimensional view of their structure with a uniform coating. The light-blue dots on the x-axis and z-axis are the magnetic-field measurement points.

1. Modeling of the pulsed sextupole magnet and the coating inside the ceramic chamber

To estimate the eddy currents generated in the coating inside the ceramic chamber of the PSM2, the elements were modeled and calculated in three dimensions by using ELF/MAGIC (ELF Corp., Osaka); this software uses the integral-element method as a feature of its code [12]. First, each magnet was assumed to have an air core and only a rectangular bar–shaped coil (see Fig. 8). These coils were placed at six symmetrical positions on concentric circles around the orbit of the stored beam to generate a sextupole magnetic field. The eddy currents on the coated surface of the ceramic chamber were generated as a reaction to the magnetic field passing through the surface; consequently, the evaluation could be simplified by using an air core and by ignoring the eddy current–induced magnetic field from the iron core. Next, a 3-μm thick uniform titanium coating was applied over the entire surface. Because the ceramic part did not need to be modeled, the coated surface consisted of two titanium plates with a width of 68 mm, a length of 300 mm, and a thickness of 3 μm, located at a vertical position $y = \pm 9$ mm from the center of the magnet ($x = y = 0$). The coating on the chamber's side surface was neglected because it does not generate a magnetic field that causes a horizontal oscillation of the stored beam. To create a pattern on the coated surface, we created a slit that simulated a comb-tooth shape in the x-direction along the z-axis to form a plate-like coating (Fig. 9). We refer to the space between coating as the slit width, which was 1 mm. Each pattern was electrically insulated at both ends along the z-axis, and eddy currents flowed only in the plane of the plate. The only magnetic field to be evaluated was that generated at the center of the chamber ($y = z = 0$) in Fig. 8 (only B_y was generated because of symmetry). The coating widths of the comb teeth varied from 5 to 10, 15, or 20 mm, with the slit width held constant at 1 mm. The eddy-current effects were compared with the case of a uniform coating (all coat) and no coating (w/o coat). Because the pulsed sextupole magnet installed in the PF ring has a single-turn coil, the adjacent coils in the figure were alternately pulsed in opposite directions (Fig. 8). The three coils of the same color in the figure are a group with the current flowing in the same direction. Next, the pulse current to the coil was set to half-sine with a pulse width of 1.2 μs and a peak current of 1000 A (Fig. 10). In the transient calculation of the magnetic field, the current was divided into 20 half-sine segments, and each step was set to 60 ns. The peak value of the current occurred at the tenth step, and the current was set to 0 A until steps 21–30. The coil material was copper.

2. Case of a uniform whole coating

In the case of a uniform whole coating, the stored beam was sandwiched between two coated surfaces without slits (Fig. 8). When the current shown in Fig. 10 was applied to this model, the temporal variation of the magnetic field in

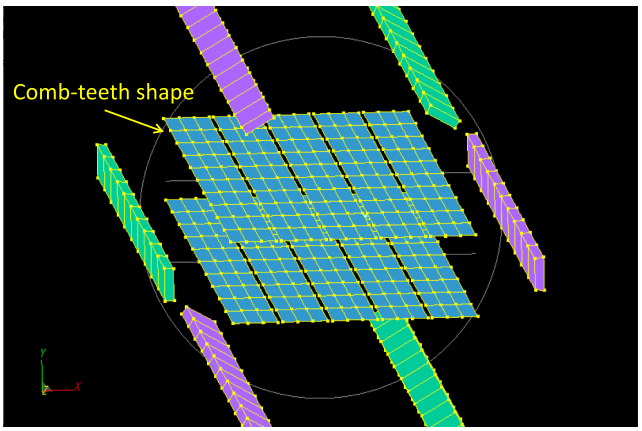

FIG. 9. Longitudinal slit model used to simulate the comb-tooth shape.

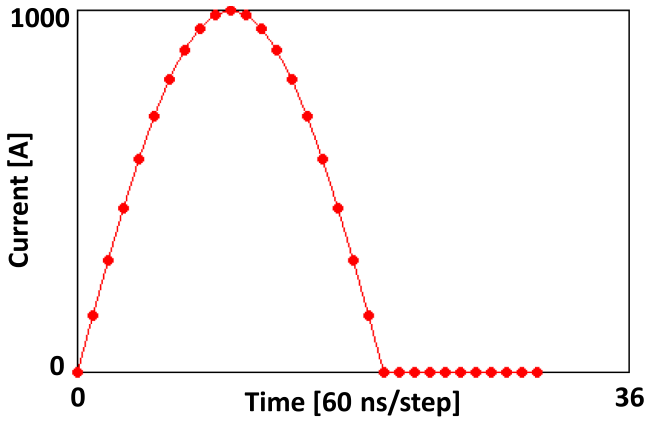

FIG. 10. Temporal evolution of the supplied current for six coils.

the measurement region shown by the dotted line in Fig. 8 changed to that shown in Fig. 11. One effect of the eddy currents is evident from the manner in which the sextupole magnetic field is generated in the x-axis direction and disappears with time. The vertical axis is normalized to 100% of the peak magnetic field generated at a horizontal position of 15 mm when no coating is present; in this case, no eddy currents are generated. The magnetic field, which should have peaked at the tenth step, peaked after a delay of two to three steps; in addition, the peak did not reach 100% because the magnetic-field strength was reduced by the eddy-current magnetic field. Another point is that the eddy-current effect appears where the opposite magnetic field is generated at a timing that cancels the sextupole magnetic field generated at a horizontal position of 0 mm when the stored beam passes through. Here, we observe the temporal evolution of the eddy-current magnetic field at $x = 0$ for the stored beam, which is similar to a sine waveform, and the effect is less than 10% of the peak value of the magnetic field for the injection beam at $x = 15$ mm in the absence of the eddy-current magnetic field.

3. *Case of a uniform whole coating with slits*

The results reported in the previous section showed that the eddy currents generated by the uniform whole coating on the inner surface of the ceramic chamber affect the stored beam. To solve this problem, a slit with a width of 1 mm was created along the z-axis of the coating in the x-direction to divide the coating into plates, simulating a comb-tooth shape (Fig. 9). First, the center line of the plate coating was placed at a horizontal position of 0 mm, through which the stored beam passes. The slits were then placed to the left and right of the coating plate, and the next coating plates were placed next to the slits. Therefore, the slits were symmetrical with respect to the horizontal position of 0 mm, and the coating (comb teeth) on the upper surfaces always faced the coating on the bottom surface inside the ceramic chamber in the vertical direction of the beam axis. We prepared coatings with four widths: 5, 10, 15, and 20 mm. Figure 12 shows the effects of eddy currents at the horizontal position of 0 mm. When a slit was cut into a coating to simulate the comb-tooth shape, the effects of eddy currents could almost be suppressed when the slit width was 5–15 mm. When the width of the slit was less than 10 mm, the effect of eddy currents was $< 1\%$ at the peak current. Figure 13 shows that the eddy currents caused a delay in the required sextupole magnetic field and a decrease in the magnetic-field strength when the uniform whole coating was applied, whereas the coating with a slit suppressed both the delay and the decrease in the magnetic-field strength.

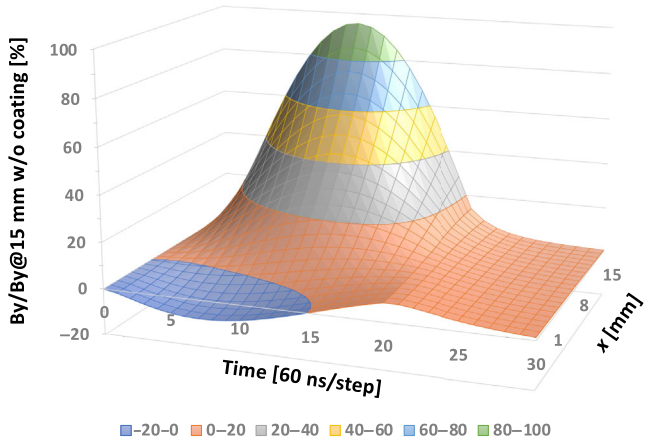

FIG. 11. Horizontal distribution with temporal evolution of the ratio between the vertical magnetic-field strength at each point in the case with a coating and the magnetic field at 15 mm in the case of no coating.

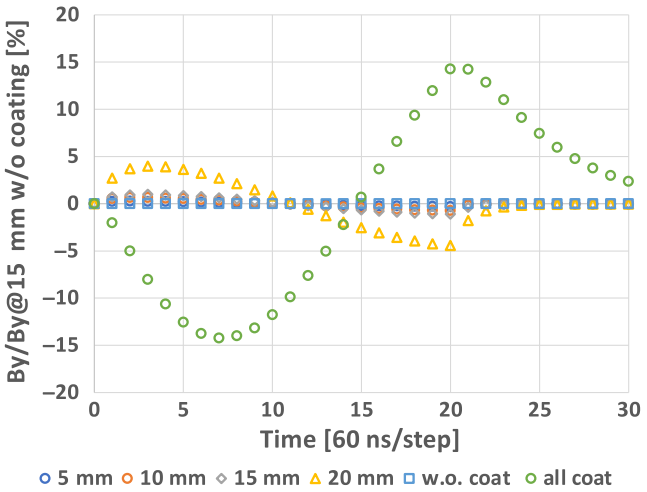

FIG. 12. Suppression of the eddy-current magnetic field at the center of the magnet, through which the stored beam passes.

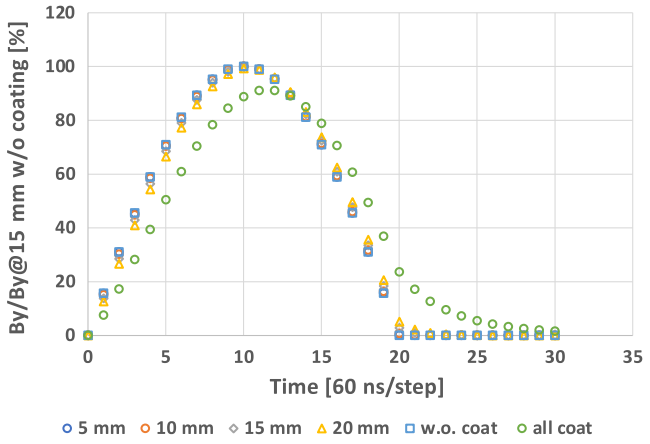

FIG. 13. The eddy-current magnetic field is suppressed at an off-center position of the magnet, through which the injection beam passes.

4. Simulation results

The optimization results based on simulations indicated that the comb-teeth width should be < 10 mm and that the loss of the main magnetic-field strength due to eddy currents should be reduced to $< 0.1\%$ in the structure in which the comb tooth was < 10 mm wide. That is, the magnetic field generated by eddy currents should be reduced by more than 99.9%.

B. Optimization for beam impedance reduction

Intuition suggests that the reduction ratio of the eddy-current effect, needed from the viewpoint of eddy-current suppression, should be maximized, whereas the beam impedance should be minimized to improve the conductivity toward the beam-wall current. To maintain a low beam-coupling impedance, the surface coverage of the inner coating should be increased. However, a uniform coating with 100% coverage is not desirable from the viewpoint of suppressing eddy-current effects. We, therefore, examined whether the impedance might be improved through capacitive coupling to compensate for the reduced coverage caused by the comb-tooth structure.

An increase in beam impedance leads directly to heat generation in the ceramic chamber. Because the ceramic chamber is covered by a magnet with a clearance of 0.5 mm, the heat generated in the ceramic chamber is not easily dissipated. If the heat generated exceeds the heat-resistance temperature of the insulation adhesive of the laminated silicon steel plates of the magnet (120°C), the magnet will not become disassembled because it is bonded by machine bolts; however, a problem would arise because the insulation between adjacent silicon steel plates would be lost, possibly resulting in the generation of large eddy currents. An increase in beam impedance is also a cause for concern in accelerator operation because it induces beam instability. Therefore, we optimized the beam impedance to

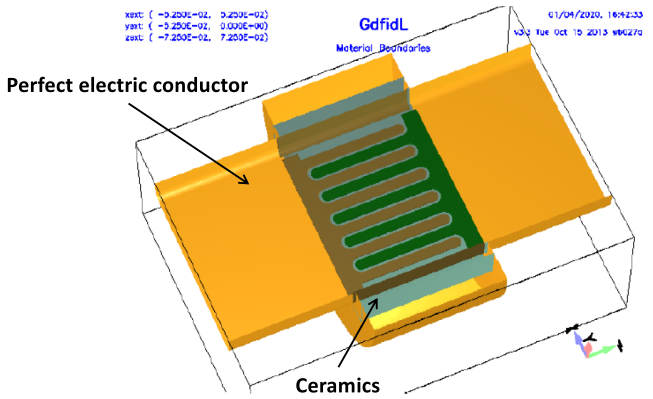

FIG. 14. Estimation by GdfidL of the beam heat generation for the pattern-coating shape of an implementation model.

be as low as possible. The boundary conditions were set to be < 70 W under natural air cooling and less than 120 W under forced air cooling, taking into account the heat-dissipation conditions.

The power loss was determined as the product of the stored-beam current, the bunch charge, and the loss factor. In the optimization, the loss factor was calculated with a simulation code by assuming a typical bunch length in the PF ring (i.e., a natural bunch length of 10 mm, assuming a Gaussian distribution). The total heat generation was calculated to achieve a total stored-beam current of 450 mA for the two filling modes: a multibunch (MB) filling mode with 188 bunches of 450 mA, and a hybrid-bunch (HB) filling mode with a single bunch of 50 mA, and 130 bunches of 400 mA. The simulation was carried out using the GdfidL code [13] through a finite-element method. The optimal comb-tooth width in terms of beam impedance was less than 4 mm, and the optimal width of the slit between the comb teeth was less than 1 mm. In the simulation, the comb teeth were placed symmetrically on the top and bottom surfaces with these basic parameters, and the loss factor was calculated (Fig. 14). In the actual coating, the comb teeth on the upper and lower surfaces were arranged to face each other asymmetrically by reversing the direction in which the comb teeth extend along the beam direction. Because the beam passes through the center of the rectangular ceramic chamber, the effects of the coating shape on the chamber sides were considered to be negligible because the sides were far from the beam. In fact, comb teeth were also applied to the sides, with asymmetrical teeth facing each other on the left and right, and asymmetrical insulation in either the upstream or the downstream direction. As such, the coating on the side of the chamber was designed so that it did not form a large ring for the vertical main magnetic field. The coverage for the entire surface coating was greater than 95%.

When this coating geometry was applied in user operations at the PF ring, the heat generated by the

MB filling mode and HB filling mode was estimated to be 20 and 67 W, respectively. In the actual HB user operation, a total beam current of 450 mA with 130 bunches of 420 mA and a single bunch of 30 mA was used to suppress the beam instabilities. The heat generated by the HB filling mode in the actual case was estimated to be 42 W. In addition, because the heat dissipation effect and forced air cooling are also considered, we concluded that there is a margin of safety in user operation. In the simulation, the coating was assumed to be a perfect conductor (500 μm) to simplify the estimation for the optimization of the geometry. The usefulness of the comb-tooth coating for beam impedance was verified in detail through actual beam experiments because of limitations in the correct estimation of the actual beam impedance for the thin coatings.

IV. FABRICATION AND BEAM EXPERIMENTS

Beam experiments were carried out to confirm whether the eddy-current effects generated in the inner surface could be suppressed by the comb-tooth coating.

A. Implementation of comb-tooth coating

In the development of the CCiPM, a FLiP coating with comb-tooth width of 2.5 mm and a slit spacing of 3 mm between the comb teeth on the inner surface of a 30 mm-diameter cylinder was produced. Therefore, we attempted to achieve the maximum allowable setting for each parameter from the viewpoint of impedance and we conducted a prototype test. The priority was to narrow the slit between comb teeth, with a target of 1 mm, without narrowing the width of the comb teeth to less than 4 mm.

Figure 15 shows the results of the pilot test, performed by using a similar process to the FLiP coating process. The width of the comb teeth at the center of the plate was wider than that on either side in this demonstration because the width optimization had not been finished at that stage. The width that was finally adopted in the actual coating was the same as the other widths. On the basis of the results of this test and demonstration, we implemented a new coating on ceramic chambers; the new chambers were fabricated during FY2019, and the fabrication and FLiP implementation of the 5 μm-thick titanium coating was successfully completed in the spring of 2020 (Fig. 16) [14]. A clear slit space of 1 mm was ensured, and the designed shape of the coating pattern was successfully implemented. Difficulties in implementing fine structures of shapes led to the delamination of some of the coatings; however, the final total surface coverage exceeded 95% and the total delaminated surface area of the coating was 0.3% of the total surface coverage. An important issue in this implementation was whether conduction paths existed between the comb teeth. Coating overlap or the presence of residue between the comb teeth would result in conduction between the comb teeth resulting, in turn, in a loss of the eddy-current suppression effect. Initially, measurements of the insulation resistance showed a value of approximately 0.3 Ω, clearly confirming the presence of conduction. In fact, the presence of points of conductivity could be confirmed visually. These conduction points were corrected and cleaned using the cleaning recipe, and an insulation resistance of 2.5×10^{10} MΩ or more between the comb teeth was finally achieved.

Before the PF ring installation, the chamber was baked at 160°C for 4 consecutive days, the achieved vacuum was 5×10^{-8} Pa and the vacuum leak rate was

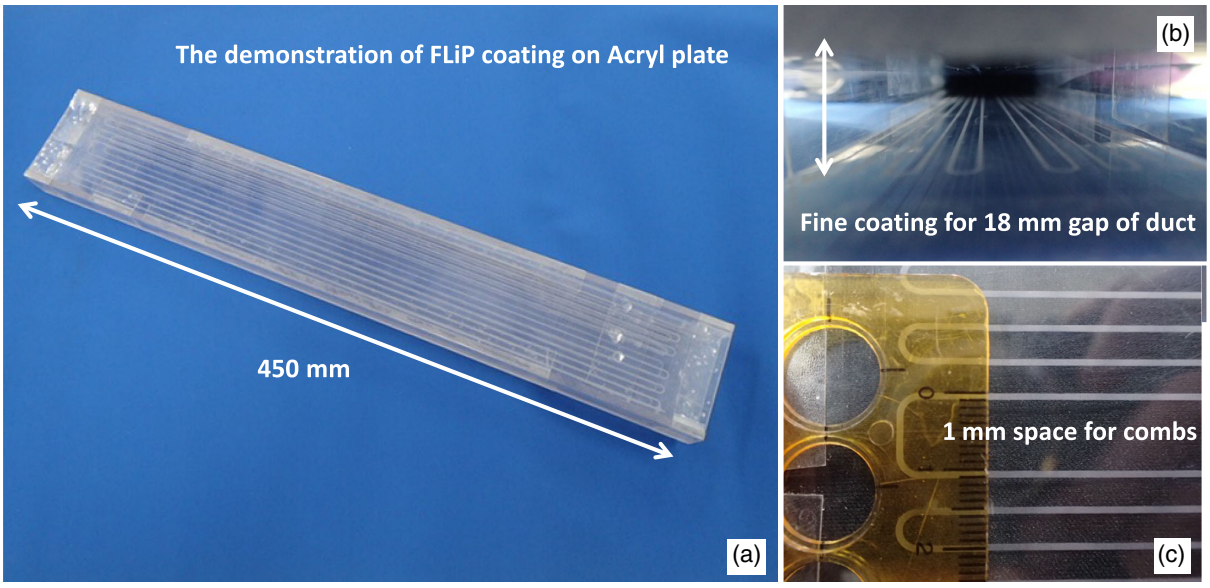

FIG. 15. Comb-tooth-patterned coating test using an acryl plate.

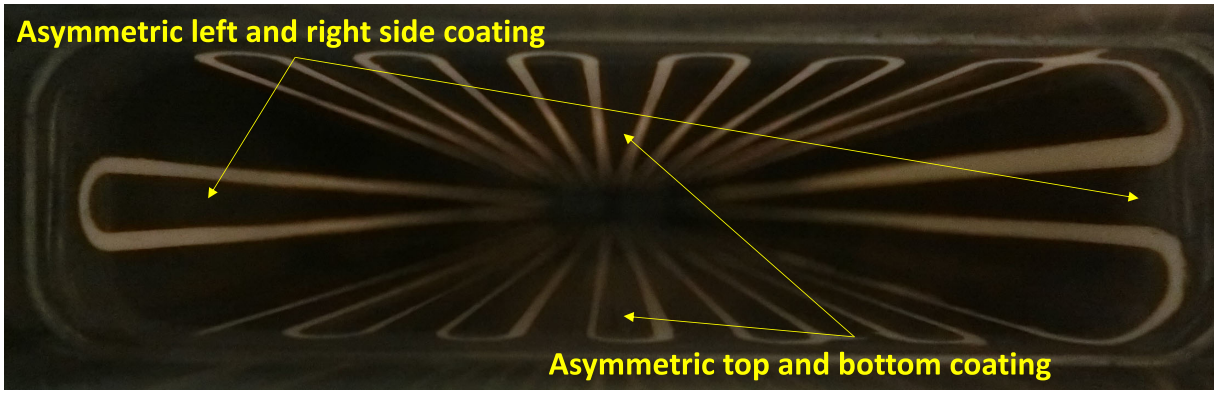

FIG. 16. Comb-tooth-patterned coating for the PSM2 ceramic chamber using FLiP technology.

$< 2 \times 10^{-11}$ Pa m^3/s. The installation was completed by the summer of 2020 for user operation starting in October 2020.

B. Heat generation in the ceramic chamber by the beam heat load

The heat generated in the ceramic chamber was carefully observed to confirm the inducement of beam instability, which was dependent on the beam-bunch filling mode. Both the MB filling mode and HB filling mode were actually tested on the ceramic chamber equipped with new coating technology. The sensor bodies of thermocouple-type temperature sensors were directly attached to the outer surface of the ceramic chamber by using Kapton tape. The total number of sensors was ten, two of which were inserted into the clearance between the magnet and the ceramic chamber in the magnet gap, whereas the others were attached to the downstream and upstream ends of the ceramic chamber. A fluorescent fiber optic temperature sensor was applied to one of the sensors inserted into the magnet gap to confirm the temperature measured by the thermocouple-type sensor. Figure 17 shows a picture taken after the temperature sensors were attached to the surface of the ceramic chamber, with the upper half of the magnet removed.

The maximum temperatures measured in the MB and HB beam filling modes were approximately 58 and 85°C, respectively; the atmospheric temperature in the accelerator tunnel was 23°C. For the HB filling mode, an air-cooling fan was used for safety after a high temperature was observed; the temperature of the fan-cooled chamber was kept below 60°C. Beam instability, which would shorten the beam life was not specially induced and was controlled under the bunch-by-bunch feedback system. In addition, the temperature generated in the single-bunch filling mode was examined for stored current from 10 to 30 mA. At a stored current of 30 mA, the maximum

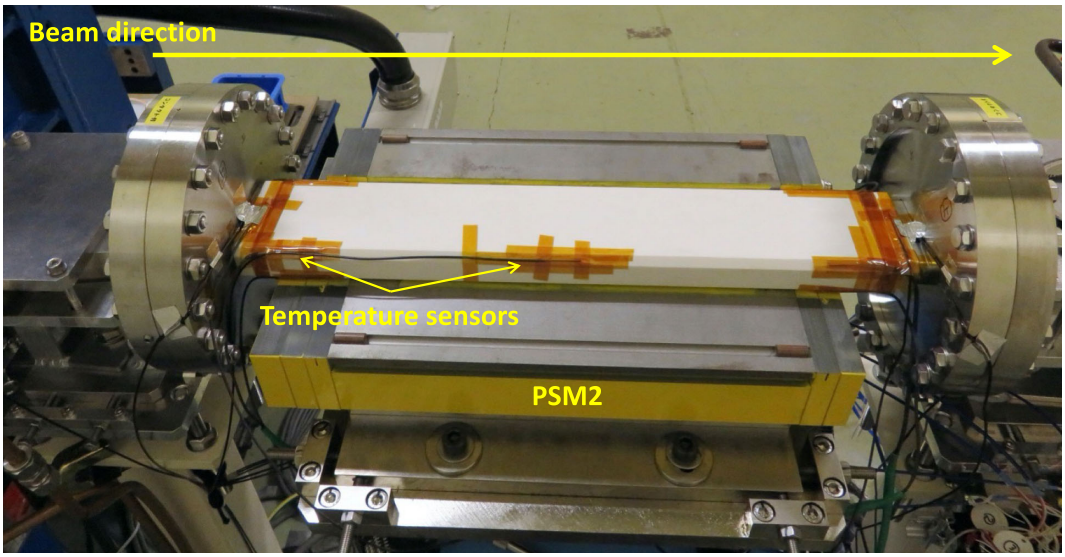

FIG. 17. Temperature sensors attached to the ceramic chamber surface to monitor the heat generated by the beam heat load.

temperature was 45°C. On the basis of the collected temperature data, the expected temperature generated for the HB filling mode was 76°C, as determined using the actual temperature results for $\Delta T = 22$°C from the room temperature for 30 mA in the single-bunch filling mode and for $\Delta T = 35$°C from the room temperature for 450 mA with 188 bunches in the MB filling mode. This value is close to the actual temperature result, corresponding to the temperature of 85°C in the HB filling mode. From these results, an estimation of the heat generation by a single bunch using the simulation code was performed before the installation of the chamber into the PF ring; this was thought to be reasonable because the result for the heat generated in the HB filling mode measured by the beam experiment was as same as that estimated by obtained by combining the temperature result for a single bunch and that for the MB filling mode in the beam experiment. The difference between the result and the expected value is speculatively attributed to bunch lengthening.

From the perspective of beam impedance, for example, a large difference exists between the calculated value and the actual result for the MB filling mode; the corresponding values are 20 and 54 W, respectively, as estimated from the actual temperature results of the heat-generation experiments, assuming that heat generation occurs on the inside surface of the ceramic chamber and that the temperature reaches equilibrium with room temperature when the heat dissipates from the magnet. This difference is speculated to result from the difference in resistivity of the coatings, as the actual titanium coating is thin whereas a thick coating with complete conductivity was assumed in the simulation.

C. Effect of the coating on stored-beam oscillation

Whereas the previous ceramic chamber was coated with a 3-μm-thick uniform layer of titanium, the new chamber carried a 5-μm-thick titanium coating with a comb-tooth pattern. Both were installed at the same location in the north straight section in the PF ring, the Twiss parameters of which are listed in Table II. The oscillations generated due to the excitation of the PSM2 were measured by using the turn-by-turn beam-position monitors placed just downstream of PSM2, and the LIBERA circuit was employed [15]. Figure 18 shows the locations of PSM2 and BPM013. The BPM can acquire the beam oscillation data for 10,000 beam revolutions. The excitation timing was adjusted to the timing at which the stored beam passed through the peak of the pulse. The initial orbit of the stored beam was corrected to pass through the center of the PSM2 by passage through the zero position at BPM013. In experiments with both the uniform surface coating and the comb tooth–patterned coating, the excitation peak current was 1000 A, so that the stored beam was not lost through collision with the beam chamber due to its large oscillation amplitude. The stored-beam oscillation during user operation should be multiplied by 2.5 times to be equivalent to the design value of 2500 A. Figure 19 shows the horizontal and vertical oscillations of the stored beam due to excitation of the PSM2, plotted as a function of the turn number. As shown in Fig. 19, the peak amplitude of the horizontal oscillation was 1.84 mm for the uniform surface coating, whereas it decreased to 0.11 mm for the comb tooth–patterned coating. Thus, the fact that the comb-tooth coating suppressed eddy-current effects to less than $1/16$ of the value with the uniform coating was confirmed by the oscillation observation experiment with the stored beam. This reduction was obtained as a result of the presence of the comb tooth–patterned coating inside the ceramics chamber, as predicted by ELF/MAGIC, and the reduction ratio of $1/16$ is reasonable, in that the eddy-current effect of the magnet remains even though the eddy-current effect of the chamber coating is suppressed completely.

TABLE II. Twiss parameters in the PF ring.

Place	$\beta(x)$ [m]	$\alpha(x)$	$\eta(x)$ [m]	Betatron phase advance/2π
Injection point	11.71	−1.301	0.667	0.000
PSM2	13.10	−0.306	0.000	1.275
BPM013	13.61	−0.369	0.000	1.284

Oscillation data with the stored-beam position shifted to ±2 mm from the center of the magnet were also acquired to confirm whether the observed beam-oscillation shape was reliable because an unexpected magnetic field is widely known to appear at ±8 mm along the horizontal axis shown in Fig. 6. Typical data for beam-oscillation shape at the center of the magnet had been confirmed to represent the effects of eddy-currents, which were, therefore, widely distributed in the region of ±8 mm. The PSM2 excitation current waveform was a half-sine with a pulsed width of 1.2 μs, which was almost twice the revolution time in the beam experiment using a new power supply. Importantly, the width of the half-sine waveform of the pulsed magnetic field observed at the off-center position beyond the ±8 mm

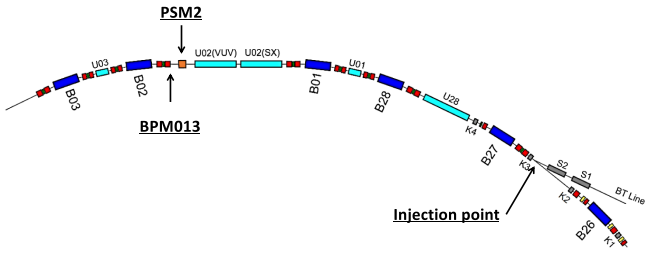

FIG. 18. Schematic view of the lattice configuration from the injection point to PSM2 in the PF ring. BPM013 was used for turn-by-turn oscillation measurements of the stored beam. The blue rectangles represent bending magnets, the red ones represent quadrupole magnets, and the light-blue ones represent undulators.

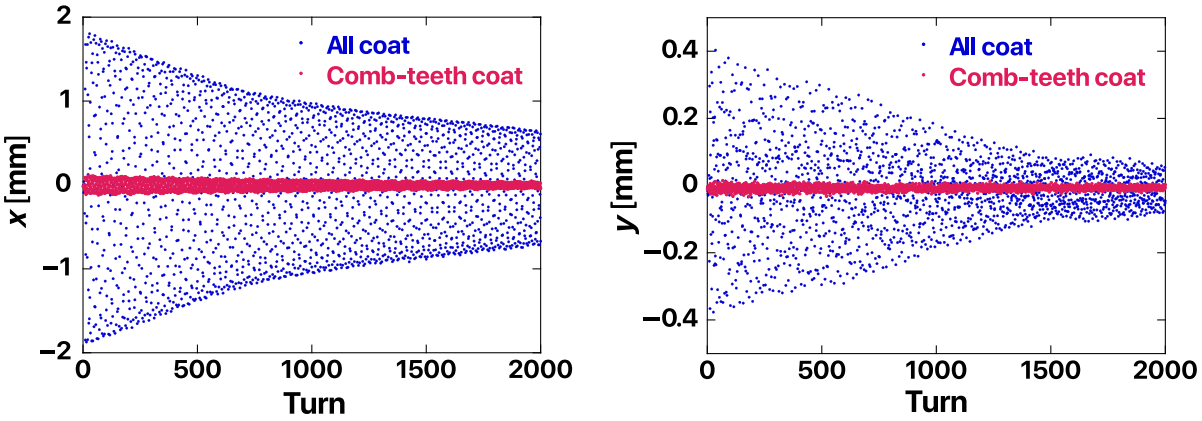

FIG. 19. Oscillation of the stored beam immediately after excitation of the PSM2 with an excitation current of 1000 A. The blue dots indicate the case where the inner surface of the ceramic chamber is fully coated (all coat); the red dots indicate the case where the inner surface is coated by the comb-tooth coating. The left- and right-hand figures show the results of horizontal and vertical beam oscillations, respectively.

region, as shown in Fig. 4, was elongated from 1.2 to 1.5 μs by the effects of eddy currents in the uniform coating of the previous ceramic chamber. In addition, the sine-like eddy-current magnetic field observed around the center of the magnet ($x = 0$) had a pulse width of 1.8 μs, as shown in Fig. 3, which is greater than the width of the half-sine waveform at 15 mm from the center of the magnet as shown in Fig. 4.

From the shape and period of the stored-beam oscillation, we can determine whether the oscillation is caused by eddy currents (sinelike) or by a sextupole magnetic field (half-sine) that includes the eddy-current effect. If the stored-beam oscillation is caused by eddy currents, the period can be used to identify whether it is an eddy current originating from the inner surface coating or from the iron core. To investigate whether an unexpected pulsed magnetic field caused by eddy currents is generated in a stored beam, we can examine the oscillation of the waveform of the pulsed magnetic field caused by the pulsed magnetic field, immediately after the generation of an eddy current, and measure the period of the oscillation. However, the interval between the nodes of the shape of the predicted eddy-current magnetic field is about 800 ns, and to observe it as an oscillation waveform of the stored beam, it would be necessary to continuously measure the bunch positions at intervals of several tens of nanoseconds by using the beam position monitor (BPM); however, it is not easy to measure the positions precisely at such intervals. To simulate this situation, the oscillations of the stored beam immediately after an eddy-current generation measured in a single bunch were superimposed by shifting the timing and these are represented as the pseudo-multibunch oscillations shown in Figs. 20 and 21.

Therefore, in both the simulated and measured data, a data set in which the electron beam is kicked at a time that coincides with the peak of the pulsed magnetic field of the

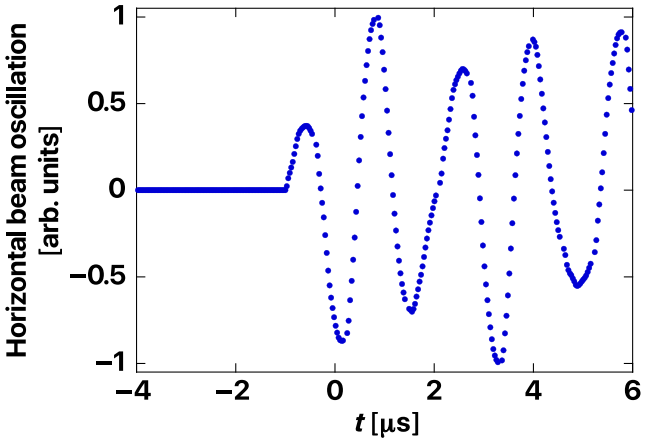

FIG. 20. Horizontal beam oscillation data for the simulated error kick by an eddy-current magnetic field.

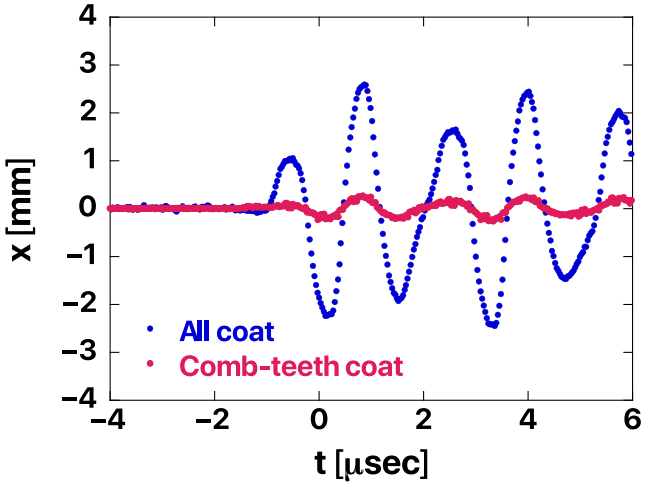

FIG. 21. Measured horizontal oscillation of the stored beam using the delayed-timing data sets in beam experiments.

pulsed sextupole magnet and another data set in which the electron beam is kicked at a time that is shifted by a step interval sufficient to permit the determination of the shape of the waveform of the magnetic field from the peak timing are repeatedly acquired. In the case when a half-period of 600 ns of a 1.2 μs-wide pulse of the magnetic field from a pulsed sextupole magnet is acquired with at 30 ns intervals, 20 data sets can be obtained. Since each of these data sets involves only a single kick for a single bunch, the data cannot be directly used to determine the shape of the waveform of the pulsed magnetic field. Instead, we have to extract the data for each revolution from the beam oscillation amplitude data in each data set and sort these data into 30-ns steps in order of delay. This analysis process creates a new data set; therefore, the data sets created from turn 1 to turn 6 can be superimposed in one figure, shifting them by one revolution time, to obtain the data shown in Figs. 20 and 21. In our measurements and analysis, the shape of the waveform of the pulsed magnetic field at the center of the pulsed sextupole magnet is determined by examining the response of a single-bunch electron beam to kicking by a magnetic field; it is then possible to simulate the oscillation amplitudes of the many electron beams that are stored in the ring in the multibunch filling mode from the results for the single bunch subjected to the unknown magnetic field.

If a uniform coating is applied to the PSM2 ceramic chamber because the stored beam is kicked by the eddy-current magnetic field with a function similar to a sine waveform with an elongated pulse width of 1.8 μs, the stored-beam oscillation should exhibit the same oscillation period as the sine waveform of the eddy-current magnetic field. To confirm whether this assumption is correct, the horizontal beam oscillation simulated by kicking by the eddy current–integrated magnetic field that was actually measured in a magnetic-field measurement is shown in Fig. 20. Observation of this oscillation period in an actual beam experiment would confirm that the stored beam is kicked by the eddy-current magnetic field measured in a magnetic-field measurement. In this beam experiment, the stored beam was passed through the center of the magnet ($x = 0$). The horizontal beam oscillation is shown for the cases of both the complete coating and the comb-tooth coating (Fig. 21). The oscillation phase in Fig 20 showing the simulation of the beam oscillation induced by the kick of the eddy-current magnetic field is consistent with the oscillation phase for the case of complete coating for an actual beam, as shown in Fig. 21. The oscillation period from node to node in Fig. 21 is 800 ns, which is approximately consistent with the half-period of the sine waveform of the eddy-current magnetic field (900 ns), as confirmed by magnetic-field measurements and by ELF/MAGIC coating simulations. That is, the shape of the eddy-current magnetic field at the center of the magnet exactly matched the beam-oscillation shape. The maximum oscillation amplitude of 2.56 mm for the ceramic chamber with a uniform coating was reduced to 0.20 mm for the ceramic chamber with a comb-tooth coating. Multiplying the oscillation amplitude of 2.56 mm by 2.5 reveals that an oscillation amplitude of 6.4 mm was achieved for the designed current supplied to PSM2 during the injection. This value is similar to the expected oscillation amplitude of 6.7 mm, based on the integrated magnetic field in the results of the PSM2 magnetic-field measurement shown in Fig. 6. The oscillation amplitude was reduced by 92%, and the oscillation period from node to node in the case of the comb-tooth coating was shortened to 700 ns from the 800 ns observed in the case of complete coating; this agreed with a reduction of the period of the sine waveform of the eddy-current magnetic field at the center of the magnet from 1.8 to 1.6 μs in the magnetic-field measurement in the absence of a ceramic chamber, as shown in Fig. 7. Therefore, the eddy-current magnetic field on the coating inside the ceramic chamber disappeared and we conclude that the remaining oscillation observed in the case of the comb-tooth coating was caused purely by the eddy-current magnetic field of the iron core, as expected on the basis of the content ratio of the eddy-current magnetic field for the iron core and coating. The experimental results, therefore, confirmed that the ceramic chamber with a comb tooth–patterned coating can be used in practical applications.

This reduction in the amplitude of the electron-beam oscillation achieved by our eddy-current suppression technique is not as good as that achieved with pulsed octupole magnets with an air-core, as promoted by BESSY II [16] and others, because the eddy-current magnetic field due to the iron core remains. In our previous study, we showed that by increasing the order of the magnetic field to an octupole, the eddy currents generated on the duct coating do not cause an unexpected magnetic field at the center of the magnet [17]. These advantages of BESSY II indicate that an air-core-type octupole pulsed magnet is more useful than an iron-core-type pulsed sextupole magnet as an injection technique. However, our results involve methods for improving eddy-current suppression in the iron-core-type pulsed sextupole magnets developed at the KEK-PF, and they show that the associated problems can be mitigated by the development of appropriate technology.

V. CONCLUSION

A PSM developed for beam injection in the PF ring is a candidate as an advanced technology for realizing the top-up beam injection without causing oscillations of the stored beam. However, the upgraded PSM system known as PSM2 did not function as expected for the PSM1 system because of an eddy current–induced magnetic field that resulted in an unexpected magnetic field around the center of the magnet. Precise magnetic-field measurements and simulations demonstrated that the eddy currents in the uniform coating and the iron core in PSM2 were the

sources of the unexpected magnetic fields around the center of magnets and that the kick angle of the integrated eddy-current magnetic field explains the beam-oscillation amplitude observed during operation of PSM2.

As a countermeasure to this problem, FLiP, a new coating technology, was developed to prevent the generation of eddy currents on the surface of the coating. The comb tooth–patterned coating realized by FLiP enabled us to confirm by simulation that the eddy-current magnetic field on the coating surface was suppressed by 99% and that the heat generation caused by the beam impedance of the wall current was reduced to within allowable levels. When the beam experiments were conducted for both the case of the uniform coating and the comb-tooth coating, the results confirmed a $1/16$ reduction of the beam oscillation.

In beam experiments, the eddy-current magnetic field was observed directly by examining the shape of the beam oscillation to prove the presence of an unexpected magnetic field due to eddy currents. The beam experiments showed that the eddy-current magnetic field on the surface of the coating was suppressed completely, which led us to conclude that the residual eddy-current magnetic field was generated in the iron core. For ultimate transparent top-up injection to a beamline user, an iron-core-type magnet is inappropriate. However, our experimental results showed that a ceramic chamber with a comb tooth–patterned coating can be used in practical applications for the next generation of light sources.

ACKNOWLEDGMENTS

The authors thank the staff of Accelerator Division VI of the Accelerator Laboratory for supporting the accelerator operation and installing the devices. In addition, the authors thank the KYOCERA special members of the PSM upgrade project, who fabricated the ceramic chamber. This work was supported by JSPS KAKENHI Grant No. 19K2649 for Scientific Research(C) in KEK and in the past by the TAKUMI project of the internal competitive fund in JASRI.

[1] T. Atkinson, M. Dirsat, O. Dressler, P. Kuske, and H. Rast, Development of a non-linear kicker system to facilitate a new injection scheme for the BESSY II storage ring, in *Proceedings of the 2nd International Particle Accelerator Conference, IPAC2011, San Sebastián, Spain*, 2011, p. 3394.

[2] Y. Hida, H. Zen, N. Yamamoto, M. Adachi, K. Hayashi, J. Yamazaki, S. Tanaka, M. Hosaka, Y. Takashima, and M. Katho, Study of pulsed sextupole magnet system for beam injection at USVOR, in *Proceedings of the 9th Annual Meeting of Particle Accelerator Society of Japan, Osaka, Japan*, 2012, p. 546 (in Japanese), http://www.pasj.jp/web_publish/pasj9/proceedings/PDF/WEPS/WEPS065.pdf.

[3] K. Ito, M. Hosaka, A. Mano, T. Takano, Y. Takashima, N. Yamamoto, K. Hayashi, and M. Katoh, Development of pulsed multipole magnet for Aichi SR storage ring, in *Proceedings of the 6th International Particle Accelerator Conference, IPAC-2015, Richmond, VA* (JACoW, Geneva, Switzerland, 2015), p. 1616.

[4] K. Harada, Y. Kobayashi, T. Miyajima, and S. Nagahashi, New injection scheme using a pulsed quadrupole magnet in electron storage rings, Phys. Rev. ST Accel. Beams **10**, 123501 (2007).

[5] H. Takaki, N. Nakamura, Y. Kobayashi, K. Harada, T. Miyajima, A. Ueda, S. Nagahashi, M. Shimada, T. Obina, and T. Honda, Beam injection with a pulsed sextupole magnet in an electron storage ring, Phys. Rev. ST Accel. Beams **13**, 020705 (2010).

[6] Y. Lu, C. Mitsuda, H. Takaki, T. Obina, K. Harada, R. Takai, Y. Kobayashi, T. Nogami, and T. Uchiyama, Evaluation of eddy current effects on a pulsed sextupole magnet by a precise magnet field measurement at KEK-PF, in *Proceedings of the 17th Annual Meeting of Particle Accelerator Society of Japan, Tokyo, Japan*, 2020 (Online), p. 363, http://www.pasj.jp/web_publish/pasj2020/proceedings/PDF/WEPP/WEPP45.pdf.

[7] A. Mochihashi, K. Yamamura, M. Hosaka, Y. Takashima, M. Katoh, M. Fujimoto, and H. Ohkuma, Perturbation to stored beam by pulse sextupole magnet and disturbance of the sextupole magnetic field in Aichi Synchrotron Radiation Center, in *Proceedings of the 9th International Particle Accelerator Conference, IPAC2018, Vancouver, BC, Canada* (JACoW, Geneva, Switzerland, 2018), p. 4232.

[8] C. Mitsuda, Y. Kobayashi, S. Nagahashi, T. Nogami, T. Obina, R. Takai, H. Takaki, T. Uchiyama, A. Ueda, T. Honiden, T. Nakanishi, A. Sasagawa, A. Yokoyama, and T. Yokoyama, Accelerator implementing development of ceramics chamber with integrated pulsed magnet for beam test, in *Proceedings of the 10th International Particle Accelerator Conference IPAC2019, Melbourne, Australia* (JACoW, Geneva, Switzerland, 2019), p. 4164.

[9] M. J. Barnes, *Proceedings of the CASCERN Accelerator School: Beam Injection, Extraction and Transfer*, Erice, Italy, 2017, CERN Yellow Reports: School Proceedings, Report No. CERN-2018-008-SP, CERN, Geneva, Vol. 5, 2018.

[10] H. Hseuh, M. Blaskiewicz, P. He, Y. Y. Lee, C. Pai, D. Raparia, R. Todd, L. Wang, J. Wei, D. Weiss, and S. Henderson, Physical and electromagnetic properties of customized coatings for SNS injection ceramic chambers and extraction ferrite kickers, in *Proceedings of the 21st Particle Accelerator Conference, Knoxville, TN, 2005* (IEEE, Piscataway, NJ, 2005), p. 3028.

[11] H. Takaki, C. Mitsuda, Y. Lu, T. Obina, R. Takai, T. Nogami, T. Uchiyama, K. Harada, A. Ueda, S. Nagahashi, and Y. Kobayashi, Evaluation of coating pattern of ceramics chambers to reduce the effect of eddy currents by the pulsed sextupole magnet, in *Proceedings of the 17th Annual Meeting of Particle Accelerator Society of Japan, Tokyo, Japan, 2020* (Online), p. 368 (in Japanese), http://www.pasj.jp/web_publish/pasj2020/proceedings/PDF/WEPP/WEPP46.pdf.

[12] http://www.elf.co.jp (in Japanese).

[13] http://www.gdfidl.de.
[14] C. Mitsuda, H. Takaki, R. Takai, T. Nogami, T. Uchiyama, Y. Lu, Y. Kobayashi, T. Obina, K. Harada, A. Ueda, S. Nagahashi, A. Yokoyama, and K. Hamaji, New installation of eddy-current suppressed ceramics duct to the pulsed sextupole magnet for top-up beam injection in KEK-PF ring, in *Proceedings of the 17th Annual Meeting of Particle Accelerator Society of Japan, Tokyo, Japan, 2020 (Online), p. 633 (in Japanese)*.
[15] https://www.i-tech.si.
[16] Patrick Alexandre, Rachid Ben El Fekih, Antoine Letrsor, Serge Thoraud, Jos da Silva Castro, Franois Bouvet, Jonas Breunlin, ke Andersson, and Pedro Fernandes Tavares, Transparent top-up injection into a fourth-generation storage ring, Nucl. Instrum. Methods Phys. Res., Sect. A **986**, 164739 (2021).
[17] Y. Lu, Development of pulsed multipole magnet for beam injection in light source, Japan, Ph.D. thesis, The Graduate University for Advanced Studies, SOKENDAI, 2022, http://id.nii.ac.jp/1013/00006252.